Available online at www.sciencedirect.com
SCIENCE DIRECT®
Physica D 199 (2004) 138–148
PHYSICA D
www.elsevier.com/locate/physd

Control of the structuring of thin soft matter films by means of different types of external disturbance

Andrey Pototsky[a,*], Michael Bestehorn[a], Uwe Thiele[b]

[a] *Lehrstuhl für Theoretische Physik II, Brandenburgische Technische Universität Cottbus, Erich-Weinert-Straße 1, D-03046 Cottbus, Germany*
[b] *Max-Planck-Institut für Physik Komplexer Systeme, Nöthnitzer Straße 38, D-01187 Dresden, Germany*

Abstract

We propose two methods to control the structuring of unstable thin films of soft matter. The first one is a non-contact method, where an external disturbance can be used to move a single drop, front or hole in a certain direction. The principle is illustrated by incorporating a sonic disturbance in a thin film equation to study the evolution of ultrathin films unstable due to their wetting properties. The second one is based on inhomogeneous templating of the substrate. Here, we study the influence of periodic modulation on coarsening in the long-time limit. Finally, the fully nonlinear evolution of a 3D system is presented by numerical integration.

PACS: 68.15.+e; 81.16.Rf; 68.55.−a; 47.20.Ky

Keywords: Liquid thin films; Nanoscale pattern formation; Fluid dynamics

1. Introduction

The creation of well-defined micro- or nanostructured thin films of soft matter attracted much interest over the last years. Unstable films on solid substrates are used in several ways to produce such patterns with defined length scale and structure. One may directly employ the surface instability by choosing the initial film thickness such that the predominant mode gives exactly the wanted length scale. However, the pattern has only a short-range order and the structure cannot be chosen independently but is also determined by the film thickness (holes, drops or labyrinths [1,2]). The evolution has to be stopped before coarsening sets in, for instance by evaporation [3] or freezing [4].

One can also use a structured substrate forcing the thin film to image it [5,6]. Contrary to (i) one needs to know the instability length scale only approximately because ideal imaging is possible in a range around it [7,8].

* Corresponding author. Tel.: +49 355 69 30 97; fax: +49 355 69 30 11.
E-mail address: pototsky@physik.tu-cottbus.de (A. Pototsky).

0167-2780/$ – see front matter © 2004 Elsevier B.V. All rights reserved.
doi:10.1016/j.physd.2004.08.019

Desirable patterns can also be obtained by manipulating the flow on the microscopic scale. This can be done by means of electrohydrodynamic pumping, electro-osmotic flow, electrowetting, thermocapillary pumping and simultaneous action of shear stress at liquid–gas interface and a variable surface energy pattern at the liquid–solid interface [9].

Here, we investigate the influence of a time- and space-periodic pressure term on thin film evolution. Practically, this can be realized by different ways. (i) One could irradiate the free film surface with ultra sound that leads to time modulation of the pressure on the liquid–gas interface. (ii) The time-periodic disjoining pressure appears in the co-moving frame of liquid films, sliding down an inclined periodically heterogeneous substrate. (iii) The use of time- and space-periodic electric field and electrowetting [10] will give rise to a time-periodic term in the total energy of the system.

The main idea behind (i), (ii) and (iii) is to create a non-uniform mean flow in a certain direction. As we showed in previous work [2], large scale mean flow may interrupt coarsening and stabilize certain periodic surface structures in the long-time limit.

In the first part of the present contribution we wish to focus on the most simple time- and space-periodic pressure term, not coupled to the film thickness which appears in case (i). Notice that a 'similar' method has been proposed in [11] and tested in [12] using light and surface tension gradients instead of sound pressure gradients on the liquid–gas interface. The second part is devoted to inhomogeneous wetting [13]. Our results are based on the thin film equation outlined in the next section.

2. Thin film equation

The spatiotemporal behavior of a thin film of incompressible liquid with a free surface on a solid smooth substrate is described by an evolution equation for the film thickness, $h(x, y, t)$, as derived from Stokes equation using lubrication approximation [14].

$$\rho\eta\partial_t h = -\nabla[\tfrac{1}{3}h^3\nabla(\sigma\,\Delta h - \partial_h f(h) - P_0)]. \tag{1}$$

where η, σ and ρ are the kinematic viscosity, surface tension, and density of the liquid, respectively. The Laplace pressure is given by $\sigma\,\Delta h$, P_0 is the gas pressure at the surface (normally assumed to be constant).

Eq. (1) has the same form as the Cahn–Hilliard equation describing the decomposition of a binary mixture [15,16]. The form corresponds to the simplest possible equation for the dynamics of a conserved order parameter field [17]. The choice of the free energy $f(h)$ determines the described physical system. It can be dewetting due to effective molecular interactions between film and substrate. Then $\partial_h f$ corresponds to the (negative) disjoining pressure and accounts for the wetting properties of the system [1,18–22]. Or it may describe a long wave Marangoni instability. Then $\partial_h f$ comes from the interaction of film thickness and temperature field [23–25]. Also combinations of both effects are studied [2]. For inclusion of other effects see the review Ref. [14].

Here, we describe ultrathin films on a solid substrate by using a disjoining pressure derived from diffuse interface theory [26,27]

$$\partial_h f(h) = \frac{2\kappa}{a}\,\mathrm{e}^{-h/l}\left(1 - \frac{1}{a}\,\mathrm{e}^{-h/l}\right) + \rho g h, \tag{2}$$

where ρ is the density of the liquid, g is the gravitational acceleration, κ has a dimension of the spreading coefficient per length, a is a small dimensionless positive parameter describing the wetting properties in the regime of partial wetting, l is the length scale of the diffuse interface [26,27]. However, note that the main results for this model will not qualitatively differ from results for other disjoining pressures combining a short-rangedestabilizing and a

long-range stabilizing component as, for example, used in [18]. This has been shown for homogeneous substrates in Refs. [21,27,28].

3. Ultrasound

To cover the first of the two driving mechanisms outlined in the introduction, we regard additionally an external sonic disturbance hitting the surface under an angle α as sketched in Fig. 1. The sonic wave breaks the isotropy of the system and is characterized by its wave length, $\lambda_s = 2\pi/k_s$, frequency, $\omega = k_s c$, wave number, k_s, and the velocity of sound in the ambient gas, c. The liquid may be considered to be incompressible if the sonic wave length is much larger than the characteristic size of the system, here the film thickness d. The pressure oscillates in the ambient gas with the sound frequency. Assuming complete reflection of the sound wave at the film surface the resulting time- and position-dependent pressure field at the film surface can be accounted for by adding to P_0 in Eq. (1) the term

$$P_s(x,t) = p\,\cos(\omega t - \phi), \tag{3}$$

where p stands for the pressure amplitude in the sonic wave. Before proceeding we shortly discuss the conditions for the sonic disturbance to be in the frame of the lubrication approximation. To obtain this conditions one has to start with Stokes equation, written for velocity and pressure fields U, P extended by small-amplitude fast-oscillating terms: $U \to U + U'(\omega t - k_s x)$, $P \to P + P'(\omega t - k_s x)$. The amplitudes of U' and P' we denote by u and p, respectively. Using the same scaling as in [14] and enforcing the final evolution equation for the film thickness h to remain its structure, we obtain the following conditions for amplitudes u and p:

$$\epsilon Re\omega\tau \ll k_s\lambda \quad \text{and} \quad \epsilon Re\omega\tau\frac{u}{U_0} \ll k_s\lambda\frac{p}{P_0},$$

where ϵ is the small parameter of the lubrication approximation, τ and λ are the time- and the x-scales, U_0 and P_0 are the characteristic velocity and pressure of the approximation, $Re = d\,U_0/(\eta\rho)$ is the Reynolds number and d denotes the mean film thickness.

The phase ϕ (defined with respect to an arbitrary wave front) at the film surface is given by

$$\phi(x, h(x)) = k_x x - k_z(h(x) - d), \tag{4}$$

where k_x and k_z are projections of the wave vector onto the x- and z-direction, respectively. The pressure distribution Eq. (3) is correct if (i) the sonic wave can reach the film surface freely, i.e. if there are no shadow regions (see Fig. 1)

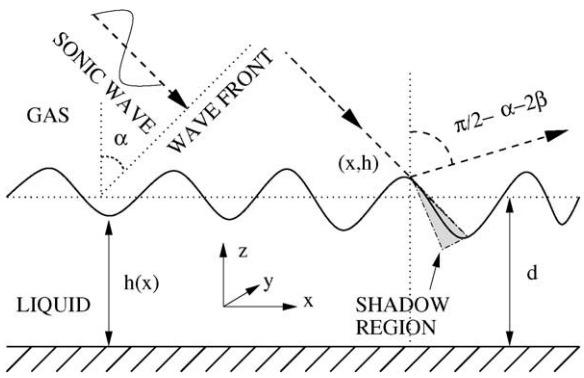

Fig. 1. Sketch of the geometry. The sonic wave is irradiated under an angle α onto the film of mean thickness d. If α is smaller than the inclination $\beta^{\text{inc}} = \arctan(\mathrm{d}h/\mathrm{d}x)$ of the surface at some point shadow regions may exist.

and (ii) if reflected waves do not fall onto the film surface elsewhere. Condition (i) is fulfilled if the angle α is larger than the maximal surface inclination of the film, $\beta_{\max}^{\mathrm{inc}}$, whereas (ii) holds if $\alpha > 3\beta_{\max}^{\mathrm{inc}}$ is satisfied. To be able to use lubrication approximation $\beta_{\max}^{\mathrm{inc}}$ has to be small. This implies that both problems are avoided if α is of order one. Then k_x and k_z are of the same order and the second term in Eq. (4) can be neglected because $d \ll L$, with L the typical scale parallel to the substrate.

Using $k_x = k_s \sin\alpha$ the pressure Eq. (3) finally writes

$$\Delta P_s(x,t) = p\,\cos(\omega t - k_s x \sin\alpha) \tag{5}$$

The system Eqs. (1) and (5) will now be used to illustrate the evolution of ultrathin films below 100 nm thickness that are unstable due to their wetting properties [14].

For $p = 0$ the linearized Eq. (1) predicts the onset of a type-IIs [1] instability at $\partial_{hh} f(d) = 0$. In the short-time regime one expects isotropic patterns with the typical wave length $\lambda_0 = 2\pi\sqrt{2\sigma/|\partial_{hh} f(d)|}$ and characteristic growth time $\tau = 12\eta\rho\sigma/d^3(\partial_{hh} f(d))^2$.

To non-dimensionalize we scale the (x, y) coordinates with $\lambda_0/2\pi$, film thickness with the mean film thickness d and time with characteristic growth time τ. Incorporating P_s, and using the same symbols now for non-dimensional variables the film evolution Eq. (1) becomes

$$\partial_t h = -\nabla[h^3\nabla(\Delta h - g(h))] + \partial_x[h^3\delta\,\sin(\Omega t - K_s x)], \tag{6}$$

with

$$g(h) = 2\frac{\partial_h f(dh)}{d|\partial_{hh} f(d)|} = 2\frac{\mathrm{e}^{-\gamma h}(1-(1/a)\,\mathrm{e}^{-\gamma h}) + \gamma G h}{\gamma|G + (2/a)\,\mathrm{e}^{-2\gamma} - \mathrm{e}^{-\gamma}|}, \tag{7}$$

and the dimensionless parameters: $G = \rho g a l/2\kappa$ and $\gamma = d/l$.

The sonic wave is characterized by the dimensionless wave vector $K_s = \lambda_0/\lambda_s \sin\alpha$, amplitude $\delta = K_s p/\sigma d(\lambda_0/2\pi)^2$, and frequency $\Omega = 2\pi\tau/T$.

The non-dimensionalization we use is suitable for the estimation of K_s and Ω. The period of the sonic wave T is much smaller than the characteristic growth time τ, so that Ω is a large number. To reach the maximum efficiency (to increase the dimensionless amplitude δ) one should use the sonic wave with smaller wavelength λ_s that will increase K_s. Of course, to justify the lubrication approximation, the sonic wavelength λ_s should be much smaller than the mean film thickness d. But if the intrinsic wavelength λ_0 is three order of magnitude larger than d (as in case of the large scale Marangoni convection [2]), one could choose $K_s \sim \lambda_0/\lambda_s = 10^1$, which does not violate the relation $d/\lambda_s \ll 1$.

3.1. Linear behavior

For $\delta \neq 0$ a flat film is not anymore a solution of Eq. (6). But one can still use linear analysis to study the initial stage of evolution. Introducing the small deviation $u(x, y, t) = h(x, y, t) - h_0$ and linearizing Eq. (6) in u gives

$$\partial_t u = -2\Delta u - \Delta^2 u + \delta\partial_x[(1+3u)\,\sin(\Omega t - K_s x)], \tag{8}$$

For $\delta \neq 0$ Eq. (8) is inhomogeneous due to the term $\delta\partial_x \sin(\Omega t - K_s x)$. Its general solution is a sum of the solution u^{H} of the corresponding homogeneous problem and a partial solution u^{I} of the inhomogeneous equation.

Using the ansatz $u(x, y, t) = \tilde{u}(x, t)\exp(\mathrm{i}\,\chi y)$ we transform Eq. (8) to

$$\begin{aligned}\partial_t\tilde{u} = {} & -\partial_x^4\tilde{u} - (2-2\chi^2)\partial_x^2\tilde{u} + (2\chi^2 - \chi^4)\tilde{u} + 3\delta\,\sin(\Omega t - K_s x)\partial_x\tilde{u} - 3\delta K_s\,\cos(\Omega t - K_s x)\tilde{u} \\ & - \delta K_s\,\cos(\Omega t - K_s x)\end{aligned} \tag{9}$$

First we wish to find the solution $\tilde{u}^{\mathrm{I}}$ of the inhomogeneous Eq. (9). To do that we use $1/\Omega$ as a small parameter and set $\tilde{u}^{\mathrm{I}} = U_{\mathrm{I}}^1 + U_{\mathrm{I}}^2 + \cdots$, where $U_{\mathrm{I}}^k \sim \Omega^{-k}$. In the first step we neglect all terms in the r.h.s. of Eq. (9) as compared with $\delta K_s \cos(\Omega t - K_s x)$. Integrating both sides over time we find $U_{\mathrm{I}}^1 = -\delta K_s/\Omega \sin(\Omega t - K_s x)$. To find U_{I}^2 we set $\tilde{u}^{\mathrm{I}} = U_{\mathrm{I}}^1 + U_{\mathrm{I}}^2$ and neglect U_{I}^2 as compared with U_{I}^1 in the r.h.s. of Eq. (9). Integration in time yields: $U_{\mathrm{I}}^2 = \delta K_s/\Omega^2[-K_s^4 + (2-2\chi^2)K_s^2 + (2\chi^2 - \chi^4)] \cos(\Omega t - K_s x)$. The amplitude of the solution $\tilde{u}^{\mathrm{I}}$ remains small if $\delta K_s/\Omega$ is a small number.

The solution of the homogeneous Eq. (9) may also be represented as a sum $U_h^1 + U_h^2 + \cdots$, where $U_h^1 = \varepsilon\, \mathrm{e}^{\beta t + ikx}$ is a small-amplitude solution ($\varepsilon \sim 1/\Omega$) of Eq. (9) in the case $\delta = 0$. The next order correction U_h^2 may be easily calculated by assuming that $\mathrm{e}^{\beta t}$ varies slowly in time T: $U_h^2 = -3\delta/\Omega[\cos(\Omega t - K_s x)\partial_x U_h^1 + K_s \sin(\Omega t - K_s x)U_h^1]$. The amplitude of U_h^2 is of order $\varepsilon/\Omega = 1/\Omega^2$.

Summarizing we may write the general solution of Eq. (8) up to terms Ω^{-2}:

$$\tilde{u} = \varepsilon \exp(\beta t + \mathrm{i}\, kx + i\chi y) - \frac{\delta K_s}{\Omega} \sin(\Omega t - K_s x) + O(\Omega^{-2}) \tag{10}$$

In the linear stage of evolution one finds a plane traveling surface wave with small amplitude, described by the second term in Eq. (10). Any infinitesimal perturbation to this plane wave (first term in Eq. (10)) has a growth rate β equal to that in the case without sonic disturbance.

As we have seen, the general solution Eq. (10) is a sum of two functions. The first one varies slowly in time, the second one is periodic with period T. The coupling between these two functions is of order $1/\Omega^2$.

3.2. Nonlinear behavior

Considering high-frequency sound one may use the averaging method [29] to derive an effective evolution equation, starting from Eq. (6). According to this method we assume the general solution of Eq. (6) to be a sum of two functions $h = \bar{h} + h'$, where $\bar{h}$ varies slowly in time and h' is some periodic function with small amplitude. Linearizing Eq. (6) with respect to h' and keeping the leading oscillating terms, we find after integration in time:

$$h' = -\frac{\delta}{\Omega}[(\partial_x \bar{h}^3)\cos(\Omega t - K_s x) + K_s \bar{h}^3 \sin(\Omega t - K_s x)] \tag{11}$$

Integrating now both sides of Eq. (6) over one period T, and keeping only the first non-vanishing term proportional to h', we obtain (after replacing $\bar{h}$ by h):

$$\partial_t h = -\nabla[h^3 \nabla(\Delta h - g(h))] - \tilde{\alpha}\partial_x h^5, \tag{12}$$

with $\tilde{\alpha} = 3\delta^2 K_s/(2\Omega)$.

Here, it is necessary to mention that the linearization and the averaging procedures do not commute. Applying the averaging method to Eq. (8) one finds that the effective evolution equation coincides with that for $\delta = 0$. So Eq. (12) is only correct in the nonlinear stage.

3.3. Numerical results

Examining (12), we recognize a similarity to the equation which describes thin liquid films on an inclined substrate [1,30]. The only quantitative difference between these two cases is the mobility factor for the driving term, which is here $Q_s(h) = h^5$ and $Q_{\mathrm{inc}}(h) = h^3$ for films on an inclined substrate. Therefore we expect the same qualitative spatiotemporal behavior: fronts and randomly distributed initial conditions may get unstable and begin to travel, driven by the sound wave. Hence, the dimensionless parameter $\tilde{\alpha}$ is suitable for estimation of order of magnitude

for the interaction of the sonic wave with the surface. Using the definitions of τ, K_s, Ω, δ one can transform $\tilde{\alpha}$ to:

$$\tilde{\alpha} = \frac{I\rho_g d\lambda_0}{2\pi\eta\rho\sigma}\left(\frac{\lambda_0}{\lambda_s}\right)^2 \sin^3\alpha,$$

where $I = p^2/(2\rho_g c)$ is the absolute intensity of the plane sonic wave, ρ_g is the density of the ambient gas.

As show the following simulations, the order of magnitude of the parameter $\tilde{\alpha}$ has to be at least larger than 10^{-4}. To reach such a value of $\tilde{\alpha}$ one has to use a very intense sonic wave with $I = 10^{-2}\,\mathrm{J/(s\,m^2)} = 100\,\mathrm{db}$ at the frequency $\omega \sim 1\,\mathrm{kHz}$, as calculated for a water film, unstable due to large scale Marangoni convection, at 60 °C with the intrinsic wavelength $\lambda = 1.64 \times 10^{-2}\,\mathrm{m}$ in the air as ambient gas layer with density $\rho_g = 1.29\,\mathrm{kg/m^3}$. The other parameters are: ($\rho = 983\,\mathrm{kg/m^3}$, $\eta = 4.7 \times 10^{-7}\,\mathrm{m^2/s}$, $\sigma = 6.6 \times 10^{-2}\,\mathrm{N/m}$).

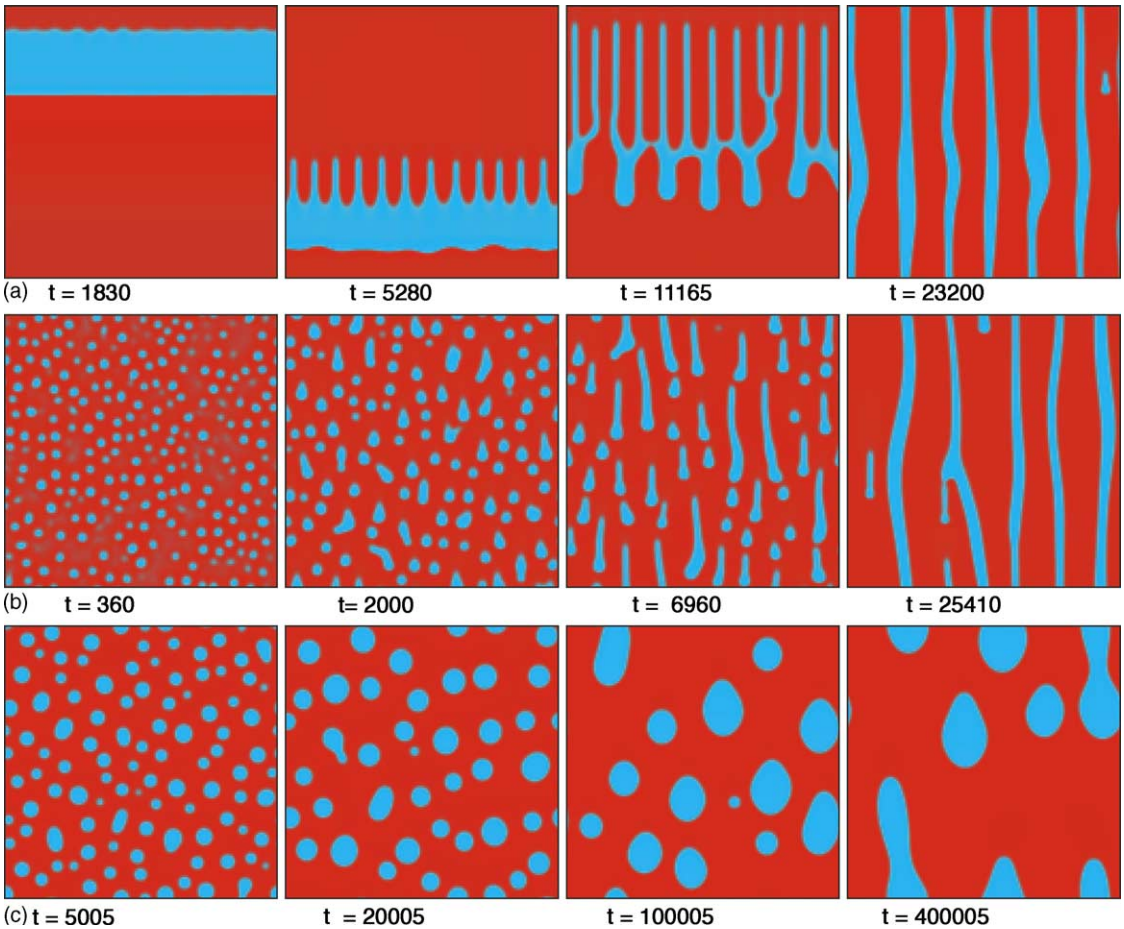

Fig. 2. Three time series found by numerical integration of Eq. (12) using different initial conditions and sound amplitudes. The direction of the sound wave is vertical. The grey scale indicates the thickness of the film, bright regions correspond to elevated parts of the surface. Parameters were $a = 0.1$, $\gamma = 1$, $G = 0.2$. (a) Instability of a front, $\tilde{\alpha} = 0.002$. In the long-time limit, coarsening is terminates and parallel stripes are stabilized. (b) The same as (a) but with a random initial condition. Now small drops are formed which merge to bigger ones and then to rivulets. Finally, the same structure as in (a) is found. (c) Drop evolution for a smaller value of the sound amplitude $\tilde{\alpha} = 0.0004$. Also here, coarsening is suppressed in the long-time limit and big drops result.

Fig. 2a and b show numerical solutions which indeed demonstrate the expected effect. We solved Eq. (12) in a two-dimensional periodic domain using pseudo-spectral code.

Note, that in the initial stage of the movement of the liquid ridge in Fig. 2a front and back become unstable independently of each other with clearly different transversal wavelengths. This corresponds very nicely to the same effect found for liquid ridges on inclined plates [1,31,32]. Therefore, it is to expect that also here with increasing driving force the transversal instability changes from an asymmetric varicose mode to an asymmetric zig–zag mode and further to decoupled front and back instability [32].

It is remarkable, that in both situations (Fig. 2a and b) coarsening is interrupted at a certain time and a structure of parallel stripes is stabilized, independent on the particular form of the initial conditions. Its final wave length depends on the force of the driving, here the square of the amplitude of the sound wave. For rather small values of the driving force, there seems to be a continuous transition to the non-driven case. Fig. 2c shows the evolution of drops as in Fig. 2b, but for $\tilde{\alpha} = 0.0004$. Also here, coarsening is suppressed in the long-time limit and big but still isolated drops result.

The drift velocity of the whole pattern strongly depends on the amplitude of the surface deflections. The drops with large amplitude drift faster than the drops on the inclined substrate due to the much stronger dependence of the mobility factor $Q_s(h)$ on the film thickness.

For practical application the plane sonic wave, irradiated to the film surface, may be of greater interest than the very slow drift on an inclined substrate. Furthermore, one can move selected parts of a pattern by using sonic waves with a spatially inhomogeneous intensity distribution (a beam of sound) For example, one may move a single drop in a desired direction.

To simulate this we consider the strength of the sonic wave to be a slow function of spatial coordinates $\delta = \delta(x, y)$ then the last term in Eq. (12) modifies to

$$\frac{3}{2}\frac{K_s}{\Omega}\partial_x[\delta^2(x, y)h^5] = \partial_x[\tilde{\alpha}(x, y)h^5].$$

The result of a simulation is presented in Fig. 3. We chose the parameters (a, G, γ) corresponding to the drop regime [1] and wait until drops are formed before we switch on the sound beam, which has a maximal amplitude in the center of the system. Its strength falls exponentially in radial direction. A drop in the center is moved towards a region where the strength of the sonic wave is weak (non-active region). After the collision of the moved drop with a drop which is in the non-active region, a curved long drop is formed. The center of the system is now free of drops.

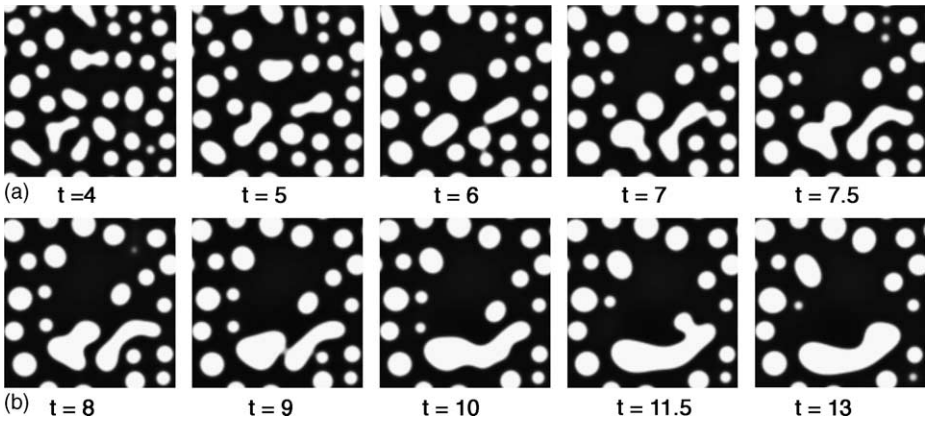

Fig. 3. Evolution of the system under the influence of a sonic disturbance with spatially inhomogeneous strength $\tilde{\alpha} = \tilde{\alpha}_0 \exp[-b((x - L/2/L)^2 + (y - L/2/L)^2)]$, where $\tilde{\alpha}_0 = 0.5$ is the strength of the sonic wave in the center of the system and $b = 25$ stands for the size of the active region. The control parameters $a = 0.1$, $\gamma = 3.5$, $G = 0.01$ correspond to the drop solution.

4. Inhomogeneous wetting

In this section, we show the influence of periodic inhomogeneities on surface pattern formation. The reason for these inhomogeneities can be different, depending on the particular system under consideration. Beneath inhomogeneously wettable substrates [13] we only mention chemically patterned substrates or space dependent heating in the case of Marangoni convection. A recent experimental work studying capillary spreading on hydrophilic stripes on a hydrophobic substrate was performed by Darhuber et al. [13].

4.1. Cahn–Hilliard equation

Since we wish to discuss the influence of inhomogeneous controlling from a more general point of view, we simplify our model Eq. (6) by assuming the system is close to its critical point [21,22,27]. We set the mobility to $Q(h) = 1$, leading to

$$\partial_t h = -\Delta(\Delta h - g(h)) \tag{13}$$

and use for g the general Taylor expansion

$$g(h) = a_0 + a_1 h + a_2 h^2 + a_3 h^3 \tag{14}$$

with the restriction for global stability $a_3 > 0$. Since only derivatives of h occur, we may shift h by a constant and rescale the coefficients in (14) to obtain $a_2 = 0$. Additional rescaling of height, time and space may lead to $a_1 = -1$ and $a_3 = 1$ if the condition for instability of the flat film is fulfilled. The most simple way to include a multiplicative modulation is to allow for spatial variation of the linear coefficient a_1. Thus, we find

$$g(h) = a_0' - (1 + \varepsilon f(x, y))h + h^3 \tag{15}$$

Inserting this into (13), we obtain the space dependent Cahn–Hilliard equation

$$\partial_t h = -\Delta h - \Delta^2 h + \Delta h^3 - \varepsilon\Delta(fh). \tag{16}$$

Without modulation, a type–IIs instability occurs with critical wave number $k_c = 1/\sqrt{2}$ and the cut-off wave number $k_m = \sqrt{2}$ [15].

4.2. Numerical results

We present time series for different harmonic inhomogeneities f. First, we use

$$f(x) = \sin(k_I x)$$

and examine its influence with respect to the wave number k_I of the modulation. From two dimensional computations [33] it is known that for wave numbers much larger than the critical one ($k_I \gg k_c$) coarsening takes place just as for the homogeneous situation. Fig. 4a show a development where $k_I = 2k_c$. Pinning is observed in the early stages, but finally coarsening dominates as for a homogeneous substrate. However, pinning is reminiscent during the whole evolution and patterns align *parallel* to the prescribed stripes.

A quite different situation occurs for a smaller wave number of the modulation. In the 2D case, pinning is expected to be dominant, which is also clearly seen in 3D. For $k_I = k_c$ the pattern organizes itself in stripes *perpendicular* to the inhomogeneity (Fig. 4b). It is also remarkable that coarsening is terminated after a certain time and a steady-state with a finite wave vector results, just as in the driven systems from the previous section.

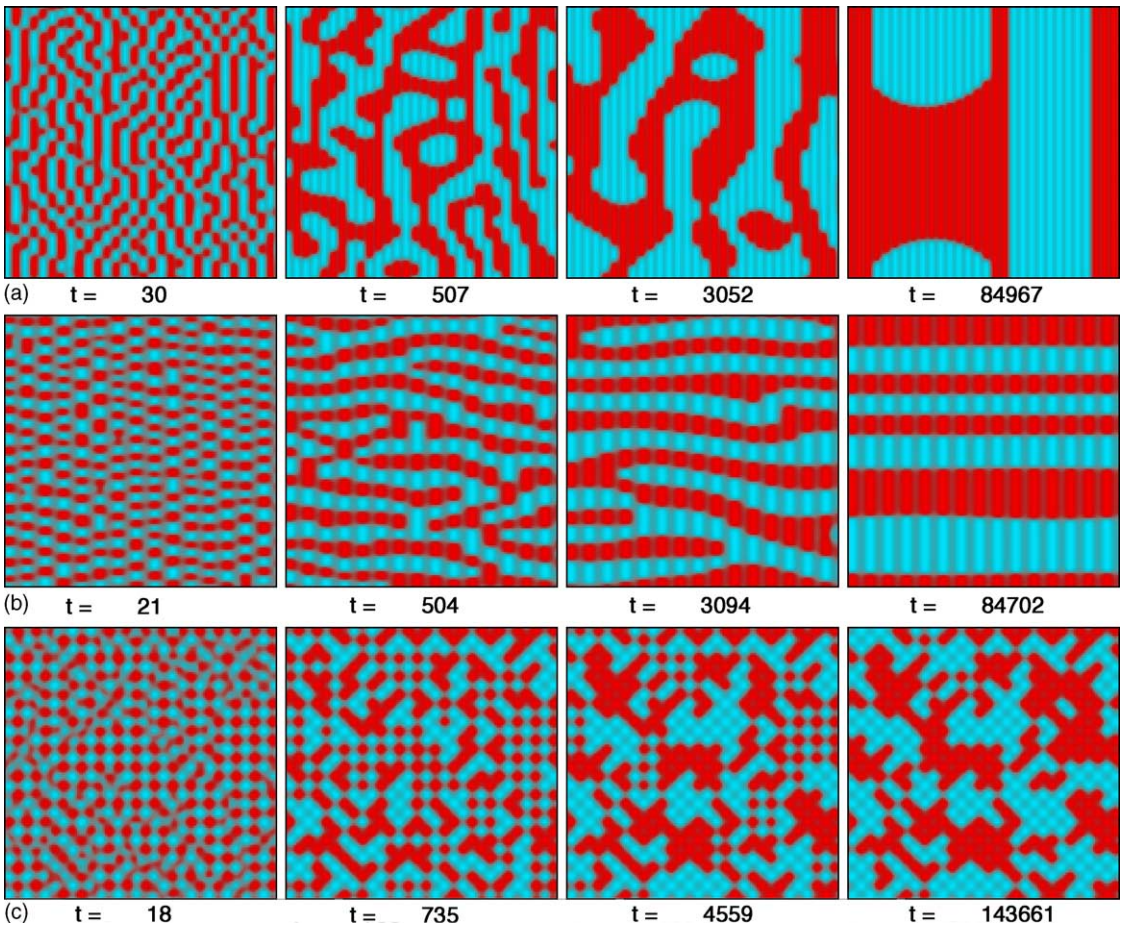

Fig. 4. Numerical solutions of the modulated Cahn–Hilliard Eq. (16) for different inhomogeneities in form of stripes (a,b) or squares (c). If the modulation wave length is much shorter than the spinodal one, coarsening dominates (a). For $k_I \approx k_c$, patterns are aligned perpendicular. Pinning on a square grid is shown in (c). The steady-state consists of filled or empty boxes.

We conclude this paragraph showing the evolution on a square-like inhomogeneity of the form

$$f(x, y) = \sin(k_I x)\ \sin(k_I y)$$

with $k_I = k_c$ (Fig. 4c). Although coarsening still exists, pinning is dominant and the fluid forms filled or empty cells on the square grid prescribed by $f(x, y)$. Such a device could store information and may be used as a "liquid memory".

5. Conclusion

The influence of external modulation on pattern formation in thin liquid films was discussed. Two different mechanisms were studied: a non-contact method using irradiation of the liquid surface with ultrasound allows for manipulation of drops, holes or fronts in a prescribed way. Moreover, spatially periodic surface structures with

desired wave length may be generated in the long-time limit. The second mechanism is based on inhomogeneous wetting properties of the solid substrate. Here, beneath the amplitude of the modulation the ratio between the two intrinsic length scales, namely the spinodal wave length and the wave length of the modulation, plays a crucial role. We showed by direct numerical integration of a model that, depending on that ratio, pinning or coarsening is the dominant dynamical behavior. The alignment of the eventually stable surface structures is also strongly influenced by this ratio.

Although both mechanisms are completely different, the resulting patterns show certain common features which have to be explored in more detail in future work. In both systems, the rotational symmetry in the horizontal plane is broken by the external modulation. This lack of symmetry expresses itself in the form of the final stable surface pattern, which turns out to be periodic in both cases. Interestingly, in both cases the surface pattern can be organized in stripes perpendicular to the external force or modulation. Coarsening, obtained always in the early stages of temporal evolution, is interrupted at a certain time and periodic patterns stabilize. The periodicity length depends thereby mainly on the strength of the external modulation.

References

[1] M. Bestehorn, K. Neuffer, Surface patterns of laterally extended thin liquid films in three dimensions, Phys. Rev. Lett. 87 (1–4) (2001) 046101.
[2] M. Bestehorn, A. Pototsky, U. Thiele, 3D large scale Marangoni convection in liquid films, Eur. Phys. J. B 33 (2003) 457–467.
[3] U. Thiele, M. Mertig, W. Pompe, Dewetting of an evaporating thin liquid film: heterogeneous nucleation and surface instability, Phys. Rev. Lett. 80 (1998) 2869–2872.
[4] J. Bischof, D. Scherer, S. Herminghaus, P. Leiderer, Dewetting modes of thin metallic films: nucleation of holes and spinodal dewetting, Phys. Rev. Lett. 77 (1996) 1536–1539.
[5] L. Rockford, Y. Liu, P. Mansky, T.P. Russell, M. Yoon, S.G.J. Mochrie, Polymers on nanoperiodic, heterogeneous surfaces, Phys. Rev. Lett. 82 (1999) 2602–2605.
[6] N. Rehse, C. Wang, M. Hund, M. Geoghegan, R. Magerle, G. Krausch, Stability of thin polymer films on a corrugated substrate, Eur. Phys. J. E 4 (2001) 69–76.
[7] K. Kargupta, A. Sharma, Templating of thin films induced by dewetting on patterned surfaces, Phys. Rev. Lett. 86 (2001) 4536–4539.
[8] L. Brusch, H. Kühne, U. Thiele, M. Bär, Dewetting of thin films on heterogeneous substrates: pinning vs. coarsening, Phys. Rev. E 66 (2002) 011602.
[9] D.E. Kataoka, S.E. Troian, Patterning liquid flow on the microscopic scale, Nature 402 (1999) 794, and references therein.
[10] T.B. Jones, M.P. Perry, Electrodynamic heat pipe experiments, J. Appl. Phys. 45 (1974) 2129.
[11] R.O. Grigoriev, Contact line instability and pattern selection in thermally driven liquid films, Phys. Fluids 15 (2003) 1363.
[12] N. Garnier, R.O. Grigoriev, M.F. Schatz, Optical manipulation of microscale fluid flow, Phys. Rev. Lett. 91 (2003) 054501.
[13] A.A. Darhuber, S.M. Troian, W.W. Reisner, Dynamics of capillary spreading along hydrophilic microstripes, Phys. Rev. E 64 (2001) 031603.
[14] A. Oron, S.H. Davis, S.G. Bankoff, Long-scale evolution of thin liquid films, Rev. Mod. Phys. 69 (1997) 931–980.
[15] J.W. Cahn, J.E. Hilliard, Free energy of a nonuniform system. Part 1. Interfacial free energy, J. Chem. Phys. 28 (1958) 258–267.
[16] J.W. Cahn, Phase separation by spinodal decomposition in isotropic systems, J. Chem. Phys. 42 (1965) 93–99.
[17] J.S. Langer, An introduction to the kinetics of first-order phase transitions, in: C. Godreche (Ed.), Solids far from Equilibrium, Cambridge University Press, 1992, pp. 297–363 (Chapter 3).
[18] A. Sharma, R. Khanna, Pattern formation in unstable thin liquid films, Phys. Rev. Lett. 81 (1998) 3463–3466.
[19] E. Ruckenstein, R. Jain, Spontaneous rupture of thin liquid films, J. Chem. Soc. Faraday Trans. II 70 (1974) 132–147.
[20] A. Oron, Three-dimensional nonlinear dynamics of thin liquid films, Phys. Rev. Lett. 85 (2000) 2108–2111.
[21] U. Thiele, M.G. Velarde, K. Neuffer, Dewetting: Film rupture by nucleation in the spinodal regime, Phys. Rev. Lett. 87 (2001) 016104.
[22] U. Thiele, Open questions and promising new fields in dewetting, Eur. Phys. J. E 12 (2003) 409–416.
[23] A. Oron, P. Rosenau, Formation of patterns induced by thermocapillarity and gravity, J. Phys. II France 2 (1992) 131–146.
[24] S.J. VanHook, M.F. Schatz, J.B. Swift, W.D. McCormick, H.L. Swinney, Long-wavelength surface-tension-driven Bénard convection: Experiment and theory, J. Fluid Mech. 345 (1997) 45–78.
[25] U. Thiele, E. Knobloch, Thin liquid films on a slightly inclined heated plate, Physica D 190 (2004) 213–248.
[26] L.M. Pismen, Y. Pomeau, Disjoining potential and spreading of thin liquid layers in the diffuse interface model coupled to hydrodynamics, Phys. Rev. E 62 (2000) 2480–2492.

[27] U. Thiele, M.G. Velarde, K. Neuffer, Y. Pomeau, Film rupture in the diffuse interface model coupled to hydrodynamics, Phys. Rev. E 64 (2001) 031602.
[28] U. Thiele, K. Neuffer, Y. Pomeau, M.G. Velarde, On the importance of nucleation solutions for the rupture of thin liquid films, Colloid Surf. A 206 (2002) 135–155.
[29] H. Schlichting, Grenzschicht-Theorie, Braun, Karlsruhe, 1951.
[30] U. Thiele, M.G. Velarde, K. Neuffer, M. Bestehorn, Y. Pomeau, Sliding drops in the diffuse interface model coupled to hydrodynamics, Phys. Rev. E 64 (2001) 061601.
[31] U. Thiele, K. Neuffer, M. Bestehorn, Y. Pomeau, M.G. Velarde, Sliding drops on an inclined plane, Colloid Surf. A 206 (2002) 87–104.
[32] U. Thiele, E. Knobloch, Front and back instability of a liquid film on a slightly inclined plate, Phys. Fluids 15 (2003) 892–907.
[33] U. Thiele, L. Brusch, M. Bestehorn, M. Bär, Modelling thin-film dewetting on structured substrates and templates: Bifurcation analysis and numerical simulations, Eur. Phys. J. E 11 (2003) 255–271.